



Orbital Debris

Quarterly News

Volume 26, Issue 2
June 2022

Inside...

| | |
|---|----|
| Additional Minor Breakup Identified in Fourth Quarter 2021 | 2 |
| ORDEM 3.2 Flux Assessment | 2 |
| SBRAM Update | 4 |
| HUSIR Radar Measurements of the Orbital Debris Environment: 2020 | 5 |
| Upcoming Meetings | 8 |
| Orbital Debris Environment Plots | 9 |
| Space Missions and Satellite Box Score | 12 |

ORDEM and MEM on the Cloud

The NASA Orbital Debris Program Office's Orbital Debris Engineering Model (ORDEM) and Meteoroid Environment Office's Meteoroid Engineering Model (MEM) are widely used by mission designers and operators (NASA, U.S. government, industry, and international) for orbital debris and meteoroid impact risk assessments. Both models are available as stand-alone, downloadable packages from the NASA Software Catalog via <https://software.nasa.gov/software/MSC-25457-1> for ORDEM or <https://software.nasa.gov/software/MFS-32205-2> for MEM.

To better serve the user community and support NASA Headquarters' Digital Transformation Initiative, MEM and ORDEM are available now as cloud-based applications. Users from around the world may benefit from this additional, easy access to the models. NASA users can access the cloud-based applications with Launchpad credentials. Non-NASA users can request access by creating an account at <https://guest.nasa.gov/>. For the cloud-based option, access ORDEM at <https://ordem.appdat.jsc.nasa.gov/> and MEM at <https://mem.mmod.appdat.jsc.nasa.gov/>. ♦

Recent Fragmentation of an Ullage Motor

The latest fragmentation of a SOZ (*Sistema Obespecheniya Zapuska*) ullage motor, or SL-12 auxiliary motor, occurred on 15 April 2022 between 05:20 and 20:33 GMT. Ullage motors, used to provide three-axis control to the SL-12's Block DM fourth stage during coast and to settle propellants prior to an engine restart, were routinely ejected after the Block DM stage ignited for the final time. The reader is referred to a prior ODQN (ODQN, vol. 18, issue 4, pp. 1-2) for an illustration and engineering drawing of a typical SOZ unit. See the SOZ Inventory Summary for the numbers of known fragmentations and units believed intact and remaining on-orbit.

This SOZ unit (International Designator 2007-065F, Catalog Number 32398), is associated with the launch of the Cosmos 2434, 2435, and 2436 spacecraft that are part of the Russian global navigation satellite system (GLONASS) constellation. The SOZ motor was in a highly elliptical 19068×400 km-altitude orbit at an inclination of 64.8° at the time of the breakup.

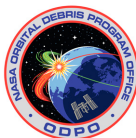
A total of 19 fragments had been identified as of 27 April; however, due to difficulties in tracking objects in deep space elliptical orbits, this event may have produced a larger fragmentation debris ensemble than has been observed to date. The likely root cause is a propulsion-related design flaw [1] leading to a fragmentation after over 14 years on orbit.

SOZ Inventory Summary

| Breakup Status | Orbital Status | | |
|----------------|----------------|-----------|------------|
| | Decayed | On-orbit | Total |
| Intact | 300 | 27 | 327 |
| Fragmented | 18 | 35 | 53 |
| TOTAL | 318 | 62 | 380 |

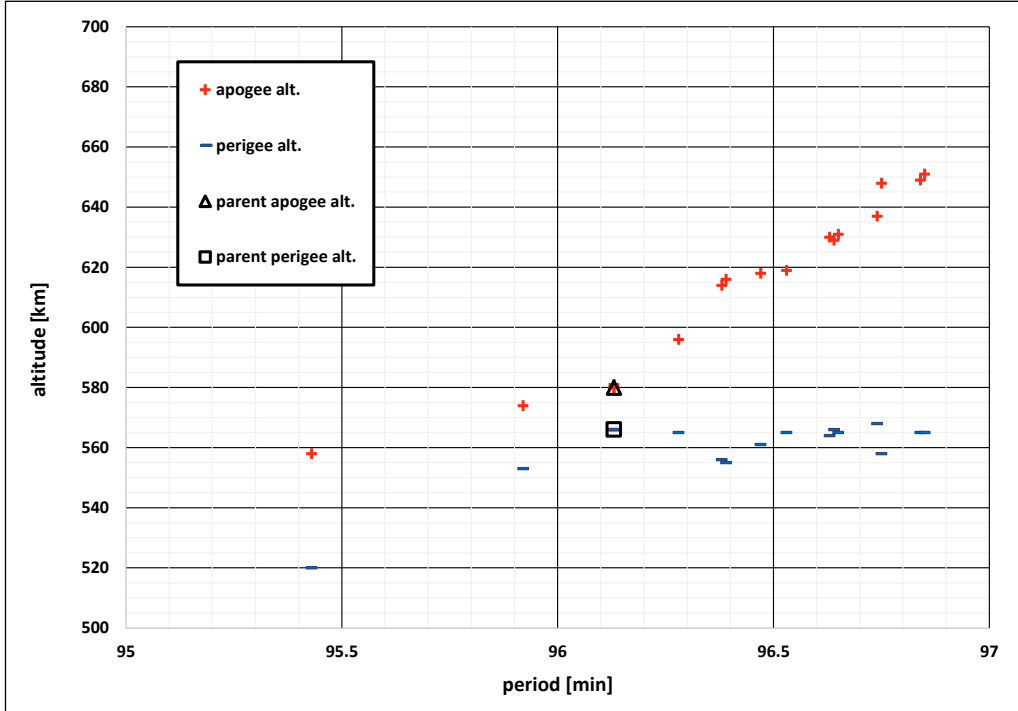
Reference

- Chernyavskiy, G.M., Johnson, N.L., and McKnight, D.S. "Identification and Resolution of an Orbital Debris Problem with the Proton Launch Vehicle," Proceedings of the First European Conference on Space Debris, ESA SD-01, pp. 575-580, (July 1993). ♦



A publication of the
NASA Orbital Debris
Program Office (ODPO)

Additional Minor Breakup Identified in Fourth Quarter 2021



The Minotaur IV fourth stage Gabbard plot. Epoch is approximately 3 April 2022. Due to the extended time between the event and its notification, four debris have reentered, and one is omitted to enhance detail of the remainder. Maximum changes in orbital parameters, for those objects with periods greater than the parent body, are 0.72 minute in period and 0.35° in inclination.

The United States Space Force's 18th Space Defense Squadron (18 SDS) noted the breakup of a Minotaur IV fourth stage that occurred on 26 November 2021 at 22:45 GMT. The vehicle (International Designator 2020-046E, Catalog Number 45877) had been on orbit approximately 1.37 years at the time of the event; approximately eight days after the event the remnant stage was observed to be in a 580×567 km, 53.98° orbit.

In addition to the parent body, 21 debris (piece tags F–AB) have entered the publicly available U.S. Satellite Catalog. A Gabbard plot of this debris cloud is presented in the figure.

The Minotaur IV fourth stage, or more generally the guidance control assembly, is built around the Orion 38 solid rocket motor, and shares a developmental heritage with the Pegasus and Minotaur I upper stages. The stage's avionics assembly includes batteries and flight termination system ordnance as well as a cold gas attitude control system in the inventory of stored energy which may have initiated the breakup processes.



PROJECT REVIEW

ORDEM 3.2 Flux Assessment

A. MANIS AND M. MATNEY

The NASA Orbital Debris Program Office (ODPO) has released the latest version of the Orbital Debris Engineering Model (ORDEM), version 3.2 (see ODQN, vol. 26, issue 1, March 2022, p. 5). ORDEM 3.2 uses the same model framework as its predecessor, ORDEM 3.1, which was released in 2019. The model has been updated to include fragments from the Cosmos 1408 anti-satellite (ASAT) test conducted by the Russian Federation on 15 November 2021. To expedite the updates to ORDEM 3.2, the underlying populations from ORDEM 3.1 were not modified, and the contributions from this breakup were added directly to this baseline environment.

The methods used for building, verifying, and validating the model populations of ORDEM 3.1 were published in NASA/TP 2022004345 “ORDEM 3.1 Model Process” and NASA/TP 20220002309 “ORDEM 3.1 Model Verification and Validation” [1, 2]. ORDEM 3.1 model populations were developed using radar, *in situ*, and optical datasets, and were then compared to datasets used for the build process as well as independent datasets for verification and validation purposes. A similar process was used for building the fragment population for the Cosmos 1408 ASAT test based on special datasets collected by the Space

Fence, the Haystack Ultrawideband Satellite Imaging Radar (HUSIR) and NASA Jet Propulsion Laboratory’s Goldstone radar (ODQN, vol. 26, issue 1, March 2022, pp. 1-5).

One design feature of ORDEM is that the flux is averaged over each calendar year. For most long-term environment evolution purposes, this is a good model choice. However, this method is not appropriate for “fresh” breakups, i.e., the short-term debris evolution from large impact events. These major events create large amounts of debris instantaneously, and some or all of the fragments can decay from low Earth orbit on time scales varying from weeks to months. For example, the total number of debris fragments from the Cosmos 1408 breakup changed significantly from November to January (see ODQN 26-1, pp. 1-5), and will continue to change over 2022 as some of the fragments drag out of orbit. To properly assess short-term risks from fresh breakups, a different modeling approach is needed. For such cases, the ODPO’s Satellite Breakup Risk Assessment Model (SBRAM) is used, as discussed in the SBRAM article on pages 4–5 in this issue of the ODQN. As the orbits of the Cosmos 1408 breakup fragments evolved in the latter weeks of 2021, SBRAM was particularly appropriate for risk calculations for assets such as the

continued on page 3

ORDEM 3.2

continued from page 2

International Space Station (ISS) and other NASA missions (ODQN, vol. 26, issue 1, March 2022, pp. 1-5).

ORDEM is intended primarily for risks projected out into the future, on timescales appropriate to spacecraft design and operations, which range from years to decades, so the decision was made not to include the Cosmos 1408 fragments in the last two months of 2021; consequently, ORDEM 3.2 has the same debris populations in 2021 as ORDEM 3.1. Otherwise, averaging in the Cosmos 1408 fragments would have entailed contributing one-eighth (the fraction of the year from November 15 to the end of December) of the cloud to the 2021 average annual flux. However, as the cloud is clearly an important contributor to the flux for 2022 and beyond, ORDEM 3.2 includes the yearly-averaged Cosmos 1408 fragments for 2022, and for later years as well. This includes averaging the ascending node and argument of perigee data of the fragments, as well as averaging the altitude contributions from individual debris as their orbits decay throughout the year. This means that, in general, ORDEM 3.2 will tend to underestimate the flux for the first part of 2022 and overestimate the flux for the latter part of 2022. However, there are exceptions to this general rule, depending on an asset's actual orbit, and ORDEM 3.2 should give a reasonable, overall estimate of the time-averaged collision risk increase from this breakup starting in 2022 and continuing into succeeding years.

Several selected orbit comparisons of the ORDEM 3.2 flux to those from ORDEM 3.1 are shown in Figures 1–3. Figure 1 shows the cumulative cross-sectional area flux for a notional ISS orbit (400 × 400 km altitude, 51.6° inclination) for the year 2022. Clearly, the primary contribution of flux increase due to the Cosmos 1408 fragments is in the 2 mm to 20 cm size range. Figure 2 shows the flux from debris with sizes ≥ 3 mm and ≥ 1 cm as a function of time for the ISS orbit. The ORDEM 3.2 flux in 2022 is approximately four and five times higher than ORDEM 3.1 for fragments ≥ 3 mm and ≥ 1 cm, respectively. The flux increase from the Cosmos 1408 fragments decreases significantly within the first few years. Note that the decrease in flux through 2027, followed by a subsequent increase, is due to solar cycle effects. Similarly, the flux

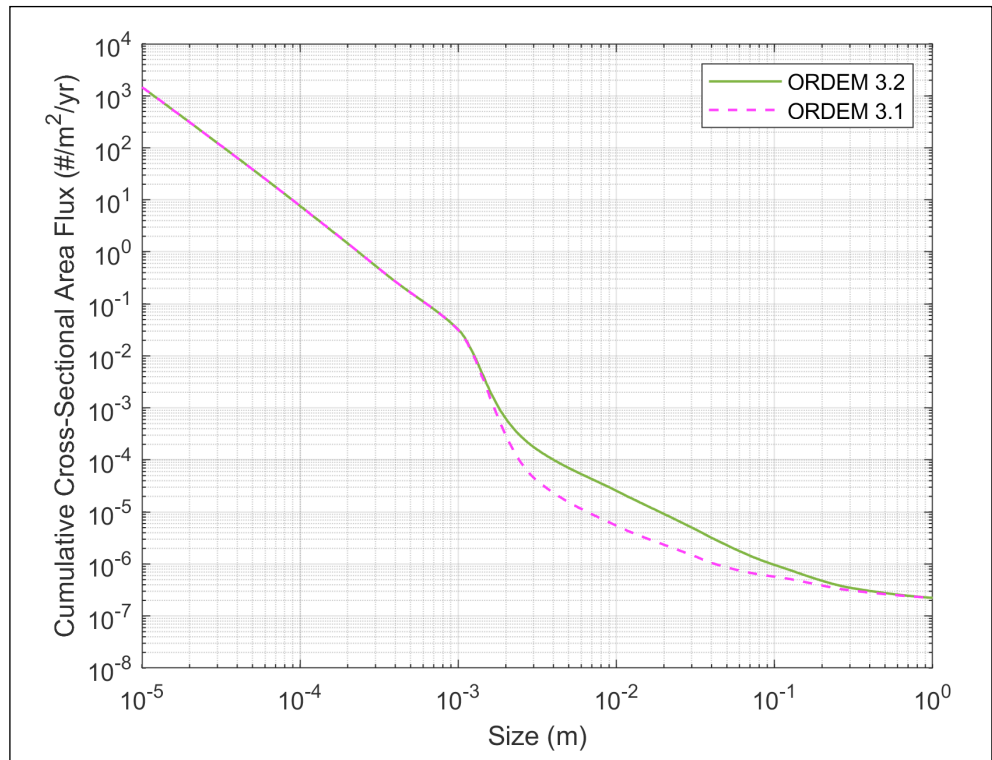


Figure 1. Comparison of the cumulative cross-sectional area flux vs. size between ORDEM 3.2 and ORDEM 3.1 for a notional ISS orbit (400 × 400 km altitude, 51.6° inclination) during the year 2022.

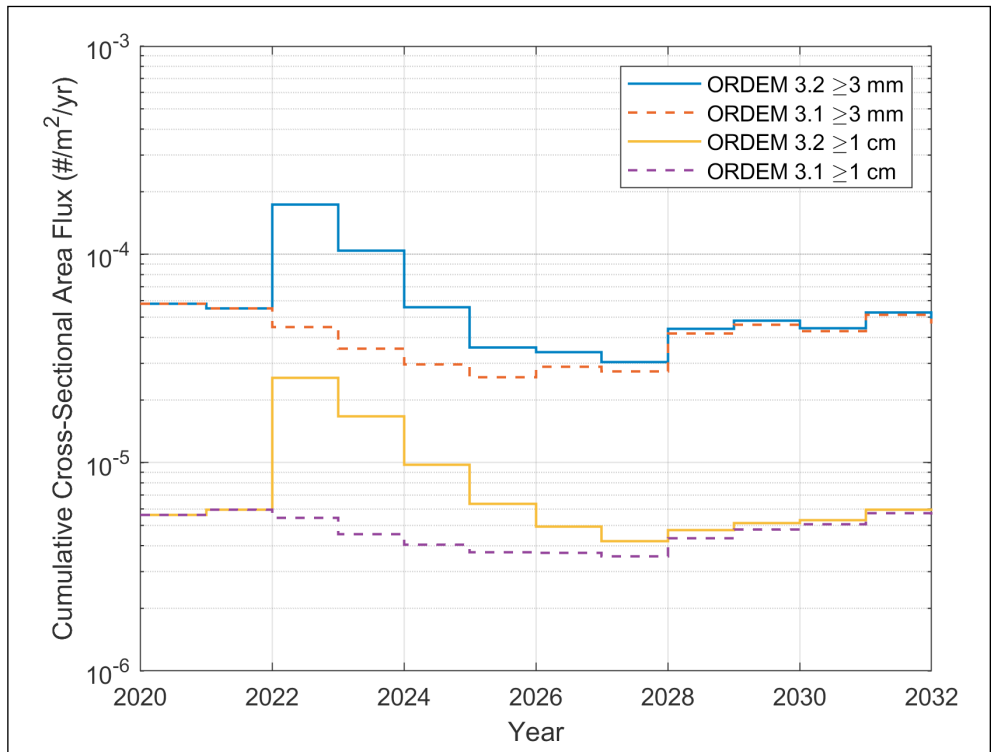


Figure 2. The cumulative cross-sectional area flux vs. time of ≥ 3 mm and ≥ 1 cm debris from ORDEM 3.2 and ORDEM 3.1 for a notional ISS orbit (400 × 400 km altitude, 51.6° inclination). Note that no additional flux was added to the 2021 average flux numbers to cover the final months of that year.

continued on page 4

ORDEM 3.2

continued from page 3

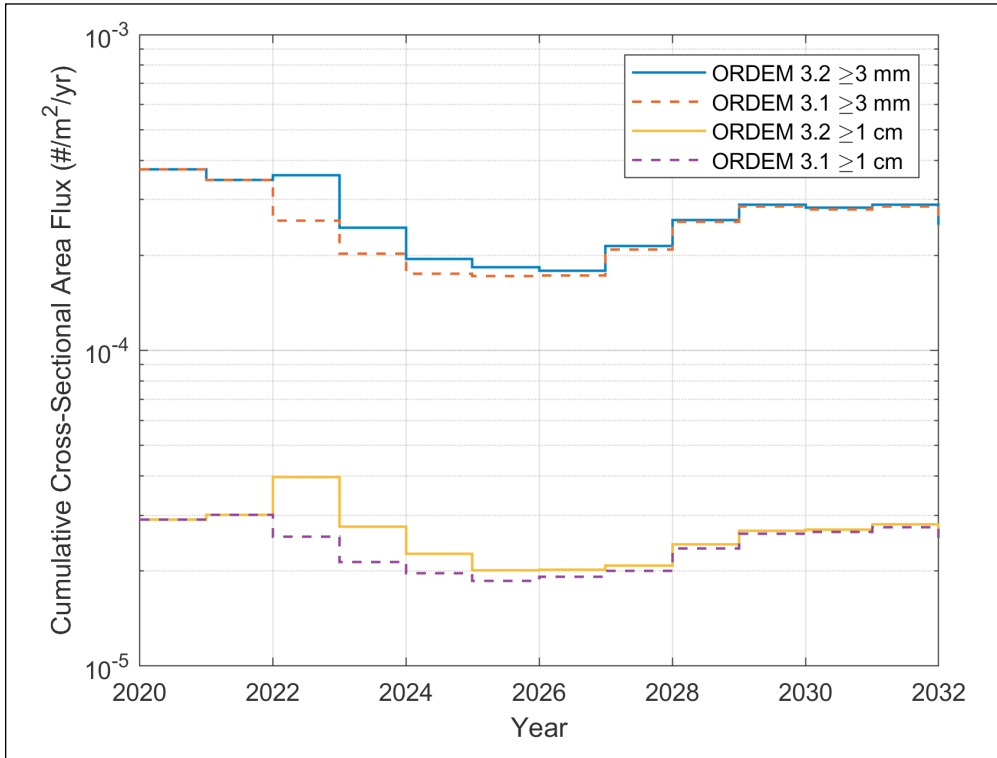


Figure 3. The cumulative cross-sectional area flux vs. time of ≥ 3 mm and ≥ 1 cm debris from ORDEM 3.2 and ORDEM 3.1 for a notional HST orbit (560×580 km, 28.5° inclination).

SBRAM Update

D. GATES AND M. MATNEY

NASA's Orbital Debris Engineering Model (discussed on pages 2-4 in this issue of the ODQN), allows a user to compute the total time-integrated flux that a spacecraft or upper stage would experience over its mission lifetime. However, users may need to assess the short-term risk from a recent breakup event where the evolution of the "fresh" debris cloud can be quite dynamic. For such cases, the Orbital Debris Program Office (ODPO) developed the in-house Satellite Breakup Risk Assessment Model (SBRAM). It was designed for computing risk assessments in the days and weeks immediately following a fragmentation event to determine whether or not specific mitigation measures are required for human spaceflight and robotic missions (see ODQN, vol. 24, issue 3, August 2020, pp. 7-11).

While continuing to calculate risk for both explosions and collisions, SBRAM 3.0 introduces an updated model that implements:

- low-velocity, fragment-asset encounters,
- asset conjunctions with ballistic fragments,
- the ability to customize each model fragment cloud (via delta-v scaling, area-to-mass ratio scaling, and scaling the number of fragments) per event, and
- the NASA Standard Satellite Breakup Model (SSBM) distributions that are fully consistent with those implemented in other ODPO software applications [1].

SBRAM simulates a discrete cloud of debris using the SSBM and propagates the debris particles deterministically under perturbations from solar radiation pressure, atmospheric drag, Earth gravitational harmonics, and lunar and solar gravity. It computes the risk to an asset by determining close approaches between it and each modeled debris piece from the SSBM. Then, SBRAM computes the actual collision probability by using a generic, Gaussian, ellipsoid probability distribution centered on each of the bodies within their respective orbits and comparing details of their conjunction-encounter geometry. The accumulation of these probabilities for each individual distribution is similar to the Gaussian Mixture Model method of mapping probability distributions. In addition to computing the probability of collision, the software preserves information on the size of the debris, the estimated time and location of the close approach within the asset's orbit, and from which directions the debris threatens the asset.

In general, the collision risk is sensitive to the initial distributions in the discrete breakup debris cloud, so SBRAM is set-up to run multiple, random cloud cases to compute average collision rates. This consists of using SSBM to create a cloud of fragments and then assigning it delta-velocity magnitudes (based on the SSBM distributions) and random directions. These velocities are then added to the parent object's velocity to produce the final, post-event, velocity vector. Each fragment is also assigned an area-to-mass ratio based on the SSBM.

continued on page 5

from fragments ≥ 3 mm and ≥ 1 cm, as a function of time, for a notional Hubble Space Telescope (HST) orbit (560×580 km, 28.5° inclination) is shown in Figure 3. For this higher altitude, the addition of the Cosmos 1408 fragments in ORDEM 3.2 leads to a slight flux increase of one to one and one-half times that from ORDEM 3.1 for ≥ 3 mm and ≥ 1 cm fragments, respectively. As with the ISS fluxes, the difference reduces to negligible levels in less than five years.

References

1. Manis, A., et al. "NASA Orbital Debris Engineering Model (ORDEM) 3.1: Model Process," NASA/TP 20220004345, (2022).
2. Kennedy, T., et al. "NASA Orbital Debris Engineering Model (ORDEM) 3.1: Model Verification and Validation," NASA/TP 20220002309, (2022). ♦

SBRAM

continued from page 4

For most conjunctions, SBRAM uses a linear approximation to compute the encounter between a modeled debris object and an asset. This assumes that the path of the high-velocity encounter over the short encounter time can be approximated as linear, which allows for simplification of the mathematics involved and speeding up of the computation time. Note that a similar technique is used to compute conjunction risk for NASA assets based on the collision warnings from the Space Force's 18th Space Defense Squadron (18 SDS). However, for certain low-velocity conjunction geometries (which typically occur when the orbits of the debris and asset are nearly coplanar), this linear approximation can cause computational problems in finding the close approach, as well as errors in the probability calculation. Therefore, an improved calculation of near-coplanar flux was derived and implemented in previous updates to the model (refer to ODQN 24-3, pg. 7).

Under certain conditions, as expected, the SSBM can produce ballistic fragments that re-enter in less than one orbit revolution. Previously, these fragments were ignored for computations, because by the time a breakup notice was provided by the 18 SDS, typically, these debris already would have decayed. However, sometimes for planning purposes, it is useful to

have this capability to compute the risk of hypothetical, or even planned breakups (*e.g.*, the USA-193 intercept, see ODQN, vol. 12, issue 2, April 2008, pp. 1-2).

The update to SBRAM 3.0 handles these encounters. For these fragments, rather than computing the close conjunctions by using the modified Simplified General Perturbations (SGP) model [2] used for orbiting objects in SBRAM, close conjunctions are computed using a modified Kepler subroutine. This method propagates the fragment over the short, ballistic arc until its reentry (ignoring the effects of Earth's gravitational harmonics).

References

1. Johnson, N.L., *et al.* "NASA'S NEW BREAKUP MODEL OF EVOLVE 4.0," Advances in Space Research, vol 28, issue 9, pp 1377-1384, (2001).
2. Hoots, F. and Roehrich, R. "SPACETRACK REPORT NO. 3 Models for Propagation of NORAD Element Sets," <https://www.celestrak.com/NORAD/documentation/spacetrk.pdf>, (1980). ♦

HUSIR Radar Measurements of the Orbital Debris Environment: 2020

J. MURRAY AND T. KENNEDY

The NASA Orbital Debris Program Office (ODPO) uses the Haystack Ultrawideband Satellite Imaging Radar (HUSIR), operated by the Massachusetts Institute of Technology's Lincoln Laboratory (MIT/LL), to characterize the distribution of debris in low Earth orbit (LEO) smaller than those typically tracked and cataloged by the U.S. Space Command's (USSPACECOM's) Space Surveillance Network (SSN), but that still represent a significant risk to human spaceflight and robotic missions. The HUSIR data collection is co-sponsored by the Space Force, but the ODPO is responsible for data processing, analysis, orbital debris environment model improvements, and model sharing. The most recent summary of these measurements is available in full detail in NASA/TP 20220006634 "HUSIR Radar Measurements of the Orbital Debris Environment: 2020" [1]. The data collected is used in the development and validation of debris populations for ODPO's Orbital Debris Engineering Model (ORDEM). An overview of the radar data collected by HUSIR is given in this review article, including recent measurement system developments and a highlight of key features of the data taken in CY2020.

The orbital debris waveform, used by HUSIR for many years, is a pulsed continuous wave with a center frequency of 10 GHz. Over the past several years, radio frequency interference (RFI) has become more prevalent at the center frequency of the debris waveform. To reduce the amount of data affected by RFI, a new waveform with a center frequency of 10.1 GHz was developed. To compare the performance of the new waveform to that of the legacy waveform, data was collected at both 10 GHz and 10.1 GHz during CY2020. Results indicate that changing the center frequency to 10.1 GHz does not negatively affect the sensitivity or beam shape of the radar and is effective at mitigating RFI. From

these results, the decision was made to permanently switch to the 10.1 GHz waveform, effective 1 October 2021. CY2020 data presented in this review contains data from both waveforms.

For orbital debris radar data collection, HUSIR operates in a "beam-park" mode in which the radar is pointed at fixed azimuth and elevation angles. Objects are then detected as they pass through the radar beam. The majority of data is collected with HUSIR pointed at 75° elevation due East; a configuration referred to as 75E. The fundamental measurements made by the radar are range, range-rate, and received power from which radar cross section (RCS) can be calculated. Figure 1 shows a plot of the range and range-rate measured for all detections, taken at 75E, for both the 10 GHz and 10.1 GHz waveforms for CY2020.

continued on page 6

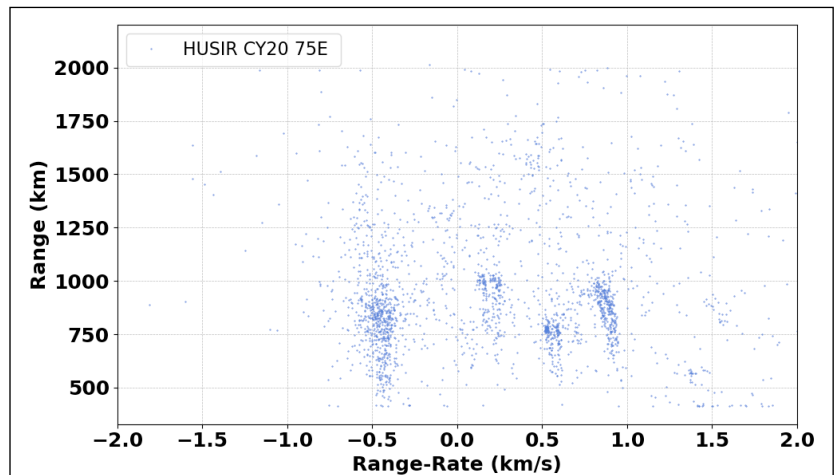


Figure 1. Range vs. range-rate observations of resident space objects, as measured by HUSIR in CY2020.

HUSIR Radar Measurements

continued from page 5

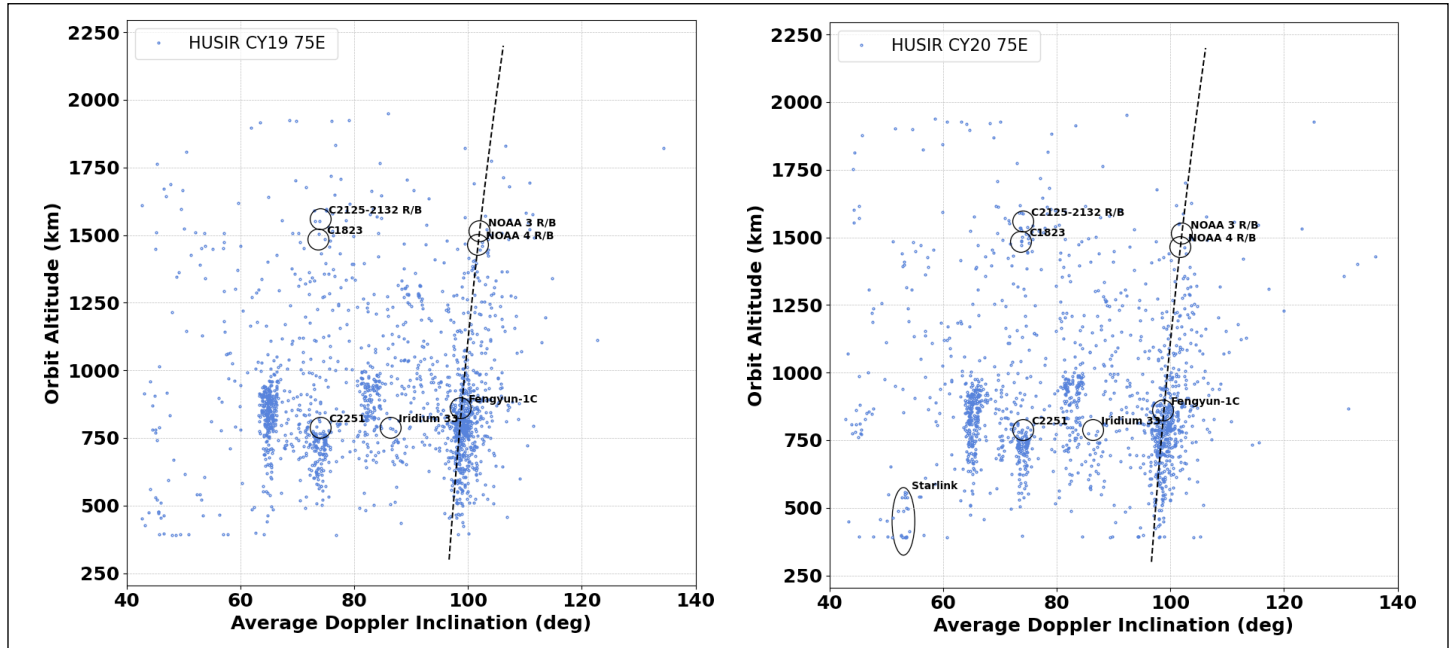


Figure 2. Conversion of HUSIR CY2019 and CY2020 range and range-rate measurements into altitude and Doppler-derived inclination. The sun-synchronous condition, assuming a circular orbit, is indicated by the dashed black line.

The orbital inclination of an object passing through the beam can be estimated using the measured range and range-rate and known pointing of the radar, if a circular orbit approximation is made for the object. Figure 2 shows the corresponding orbit altitude and inclination of detections made in CY2020, as well as CY2019 for comparison purposes. When viewed in this way, distinct families of debris become apparent. Figure 2 also highlights some notable on-orbit fragmentations with black circles, where the center of the circle represents the altitude and inclination of the parent body at the time of the event [2]. The altitude-inclination relationship of the sun-synchronous condition for circular orbits is shown as a dashed black line [3].

Additionally, a black ellipse highlighting a new minor grouping of

detections is shown near 53° inclination: one at an altitude of 550 km and the other at 392 km, the latter altitude corresponding to the lower range-window limit of the radar waveform used. These groupings are more readily apparent when comparing to data from CY2019. Note that Doppler inclination estimates for detections at or below the range window limit will exhibit some spread due to error in the measured range, and the new cluster at this lower altitude appears to be spread over more Doppler inclinations as a result. This new family of detections is associated with the increased satellite traffic associated with Starlink. By the end of CY2020, SpaceX deployed 833 Starlink satellites to 550 km altitude and 53° inclination orbits. Starlink satellites also have a “checkout orbit” after launch of about 350 km, which may manifest as 392 km in the data due to HUSIR’s range window. Additionally, a second fragmentation of a *Fregat* upper stage debris object previously identified as “SL-23 DEBRIS,” (International Designator 2011-037B, Catalog Number 37756) occurred near this inclination in CY2020.

The RCS of an object is calculated using the measured power of the reflected signal and the range of the object. The size of a debris object can be estimated from the RCS using the NASA Size Estimation Model (SEM) [4]. Figure 3 shows a plot of altitude versus SEM-estimated size for HUSIR detections. Also included are curves that represent the altitude-dependent size to which the data is estimated to be 99%, 95%, and 90% complete. These correspond to 6 mm, 5.8 mm, and 5.7 mm, respectively, at 1000 km altitude. A comprehensive description of the estimation method is given in [1].

Figure 4 shows the cumulative count rate versus SEM-estimated size for each year between CY2018 through CY2020, limited to less than 1000 km altitude and smaller than 10 cm. The 10 cm limit was chosen to avoid variations

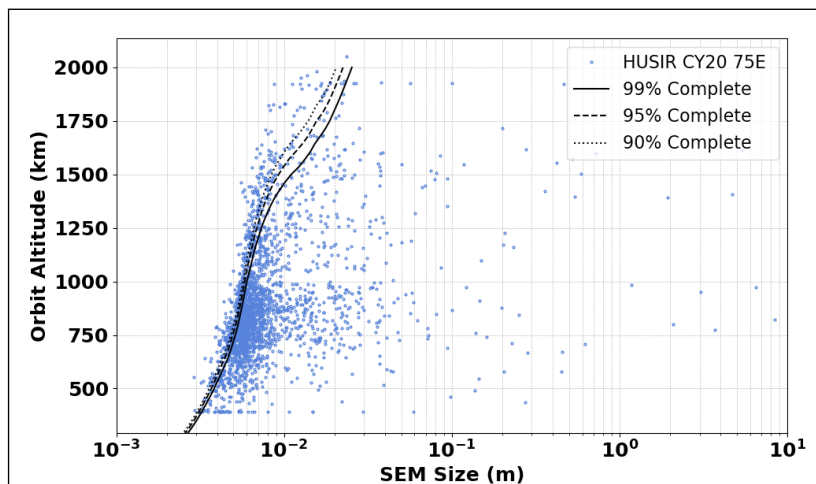


Figure 3. Orbit altitude vs. SEM size for HUSIR CY2020 75E data at 10 GHz with 99%, 95%, and 90% completeness curves as a function of altitude.

continued on page 7

HUSIR Radar Measurements

continued from page 6

in the distribution of large objects that skew the distribution at smaller sizes and corresponds to the size to which the SSN catalog is estimated to be complete. Note that the variations in the distribution of large objects is the result of sparse counting statistics using HUSIR for this population.

The Indian spacecraft Microsat-R (International Designator 2019-006A, Catalog Number 43947), was intentionally destroyed in a test of a ground-based, direct-ascent anti-satellite (ASAT) weapon system in CY2019, resulting in HUSIR measuring an increased debris flux at altitudes below 600 km. Using a model of the debris cloud generated with the NASA Standard Satellite Breakup Model, it was possible to flag a subset of detections in the CY2019 data as likely being correlated to the Microsat-R debris [5]. These flagged detections were removed from the data to produce the CY2019 distribution shown in Figure 4 and to better compare the background debris environment between years. Neglecting differences in the roll-off region at the smallest sizes detectable by the radar, due to sensitivity differences, the CY2020 cumulative size distribution, aggregated over all altitudes and inclinations, is statistically equivalent to previous years. However, statistically significant changes in flux localized to particular altitudes and inclinations have been observed.

In addition to total cumulative-count rate, it is important to monitor debris flux variations in altitude regions of interest. In particular, characterization of the on-orbit lifetime of small fragments produced by the Microsat-R ASAT breakup event is of interest. Initial analysis of the low-altitude flux observed in CY2019 showed the increase starting in the second quarter (Q2) of CY2019 – just after the fragmentation event – and remaining elevated into Q3. By Q4, the flux increase showed signs of subsiding.

Figure 5 shows the flux from 400 km to 525 km altitude from U.S. Government fiscal years FY2014 through FY2017 and CY2018 through CY2020, limited to the 99% completeness size of 6 mm for CY2020. It should be noted that the detections flagged as Microsat-R in CY2019, which were not considered in Figure 4, are present in this comparison. An upper altitude of 525 km was chosen to exclude the unrelated 550 km-altitude increase seen in CY2020. The distinction between FY and CY comes from a change in the basis of data reporting that occurred from FY2017 to CY2018. Each datapoint and estimated uncertainties covers one year without overlap in time. The figure shows that the low altitude flux in CY2020 continues to decrease toward background levels and indicates that the effects of the Microsat-R ASAT test on the small particle environment in LEO were only short term.

This high-level summary of HUSIR CY2020 orbital debris measurements was presented, focusing on the contributions from Microsat-R, comparisons between different years (CY and FY), and additional clusters at 53° inclination from Starlink traffic. A new waveform, effective at the mitigation of RFI, was developed and validated for future use to ensure that more usable observation hours can be obtained from HUSIR measurements. Ongoing observations of the debris environment remain necessary to develop accurate debris environment models.

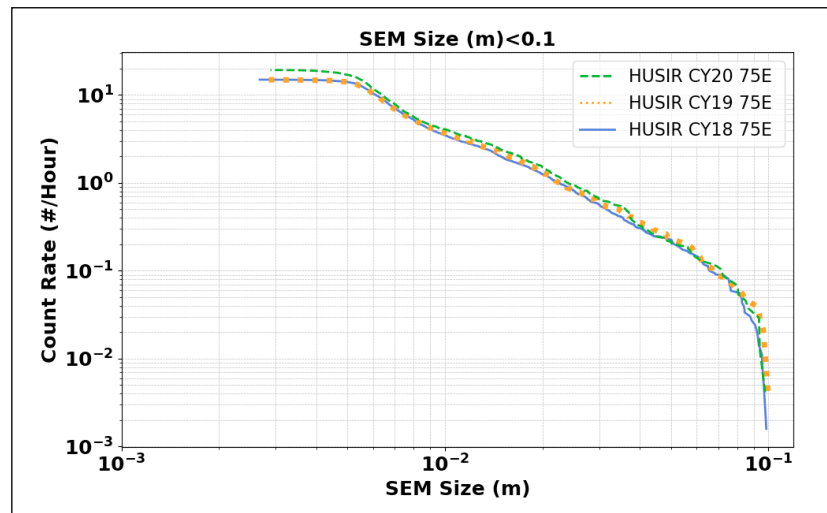


Figure 4. Cumulative count rate as a function of SEM-size for objects below 1000 km in altitude and smaller than 10 cm in size, with Microsat-R associated debris removed for background comparison.

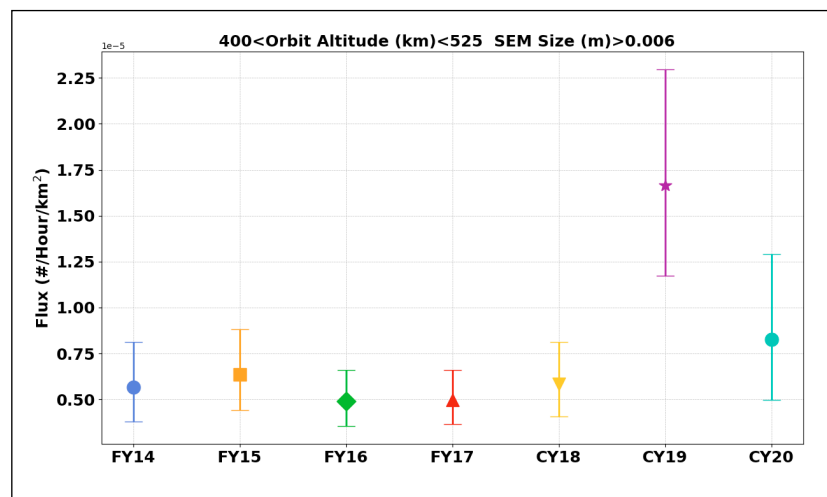


Figure 5. Surface area flux between 400 km and 525 km in altitude limited to ≥ 6 mm for all 75E data by year. The error bars represent the 95% Poisson confidence intervals.

References

1. Murray, J. and Kennedy, T. "Haystack Ultrawideband Satellite Imaging Radar Measurements of the Orbital Debris Environment: 2020," NASA/TP 20220006634, May 2022.
2. Anz-Meador, P.D., et al. "History of On Orbit Satellite Fragmentations," 15th Edition, NASA/TM-2018-220037, (2018).
3. Vallado, D.A. Fundamentals of Astrodynamics and Applications, 4th Edition, Microcosm Press, pp. 862-869, (2013).
4. Xu,Y.-L., et al. A statistical size estimation model for Haystack and HAX radar detections, IAC-05-B6.1.02, 56th International Astronautical Congress, 2005
5. Murray, J. and Kennedy, T. "Haystack Ultrawideband Satellite Imaging Radar Measurements of the Orbital Debris Environment: 2019," NASA/TP-20210013669, April 2021. ♦

UPCOMING MEETINGS

These events could be canceled or rescheduled due to the COVID-19 pandemic. All information is current at the time of publication. Please consult the respective websites for updated schedule changes.

18-22 September 2022: 73rd International Astronautical Congress (IAC), Paris, France

The IAC will convene in-person in 2022 with a theme of “Space for @ll.” The IAC’s 20th IAA Symposium on Space Debris will cover debris measurements and characterization; modeling; risk analysis; hypervelocity impact and protection; mitigation; post-mission disposal; space debris mitigation and removal; operations in space debris environment; political and legal aspects of including mitigation and removal; orbit determination and propagation; and a joint session on near Earth objects and space debris. The abstract submission has passed. Additional information for the 2022 IAC is available at <https://www.iafastro.org/events/iac/iac-2022/> and <https://iac2022.org/>.

18-22 September 2022: 16th Hypervelocity Impact Symposium, Alexandria, Virginia, USA

The Hypervelocity Impact Symposium (HVIS) is a biennial event organized by the Hypervelocity Impact Society that serves as the principal forum for the discussion, interchange, and presentation of the physics of high- and hypervelocity impact and related technical areas. Orbital debris-related presentations include fracture and fragmentation; launchers and diagnostics; penetration mechanics and target response; hypervelocity phenomenology studies; material response; meteoroid and debris shielding and failure analysis; theoretical applied mechanics relevant to hypervelocity impact; and a special session on state-of-the-art experiments enabling advances in state-of-the-art models. The abstract submission deadline has passed. Additional information for the 16th Symposium is available at <http://hvvis2022.jhuapl.edu/>.

27-30 September 2022: 23rd Advanced Maui Optical and Space Surveillance Technologies Conference, Maui, Hawaii, USA

The technical program of the 23rd Advanced Maui Optical and Space Surveillance Technologies Conference (AMOS) will focus on subjects that are mission critical to Space Situational Awareness. The technical sessions include papers and posters on Orbital Debris; Space Situational/Space Domain Awareness; Adaptive Optics & Imaging; Astrodynamics; Non-resolved Object Characterization; and related topics. The abstract submission deadline has passed. Additional information about the conference is available at <https://amostech.com>.

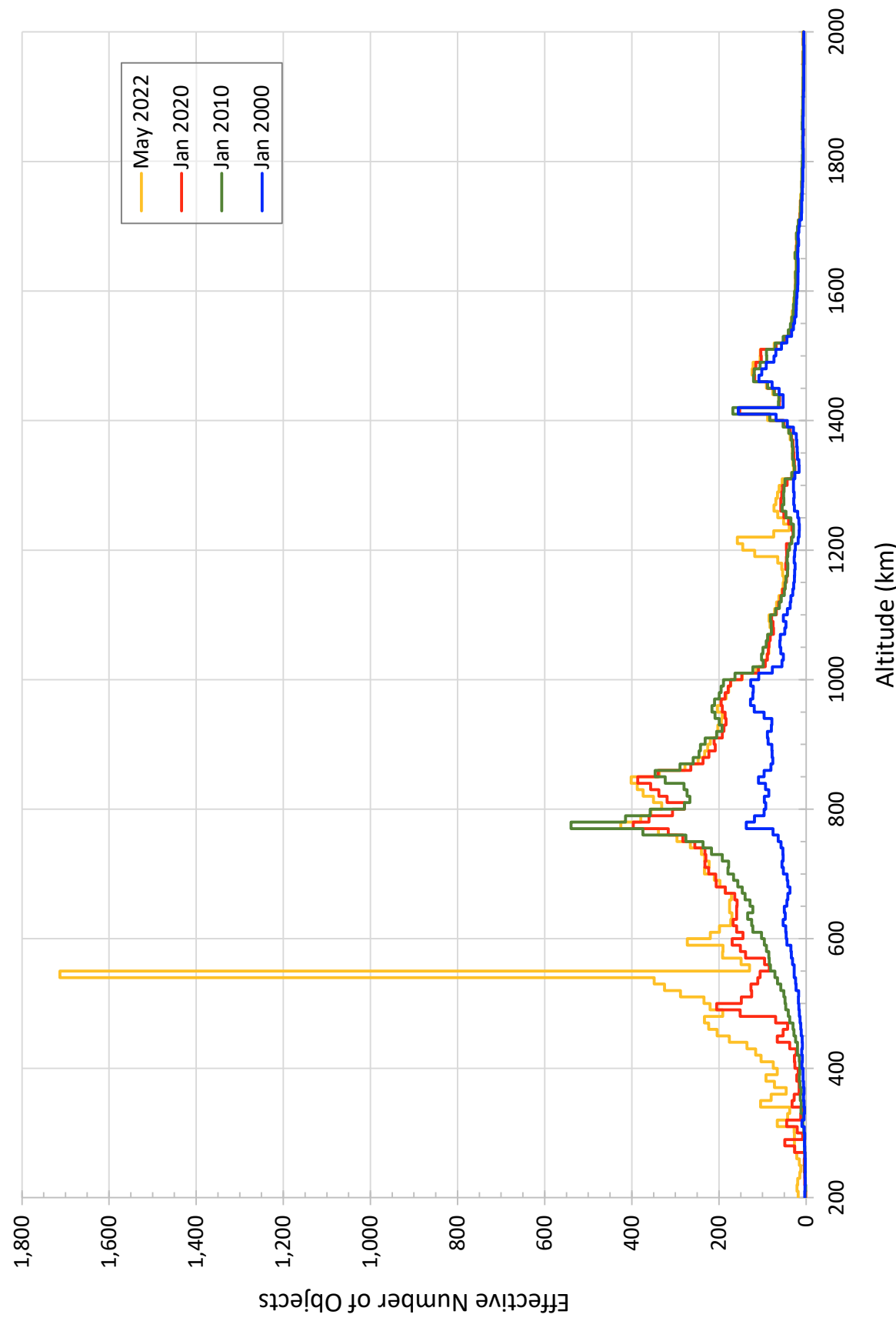
Orbital Debris Modeling Scientist Job Postings

The NASA Orbital Debris Program Office (ODPO) is looking for candidates to support radar/optical/in-situ/laboratory data analyses and associated orbital debris environment modeling. If you or a colleague is interested in working with the primary contractor for ODPO, please see the hyperlinks below. The positions are posted at different levels depending on education and experience.

Click each link provided to see the complete job description.

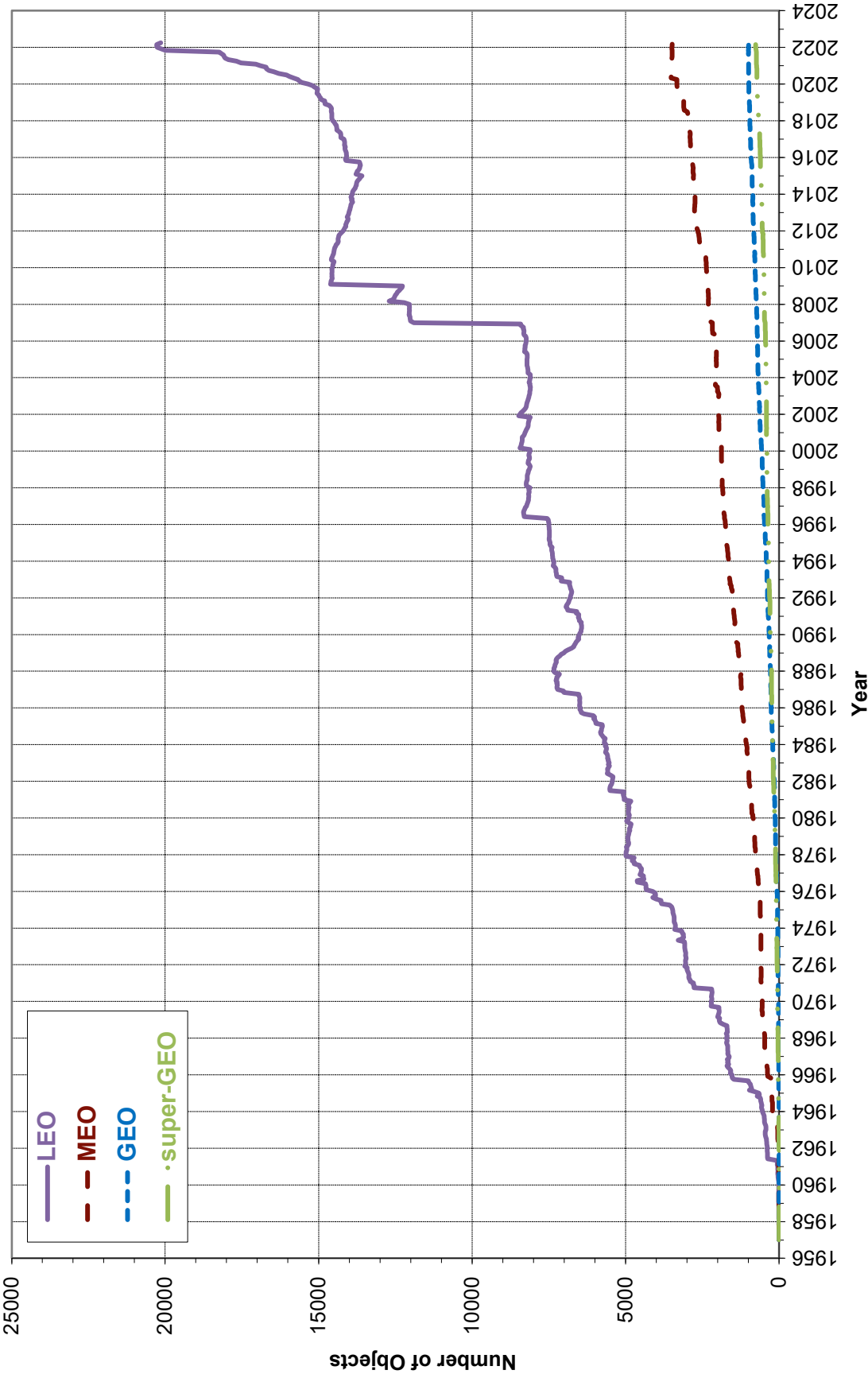
<https://jacobs.taleo.net/careersection/ex/jobdetail.ftl?job=ADV0002MP>

<https://jacobs.taleo.net/careersection/ex/jobdetail.ftl?job=ADV0002MQ>

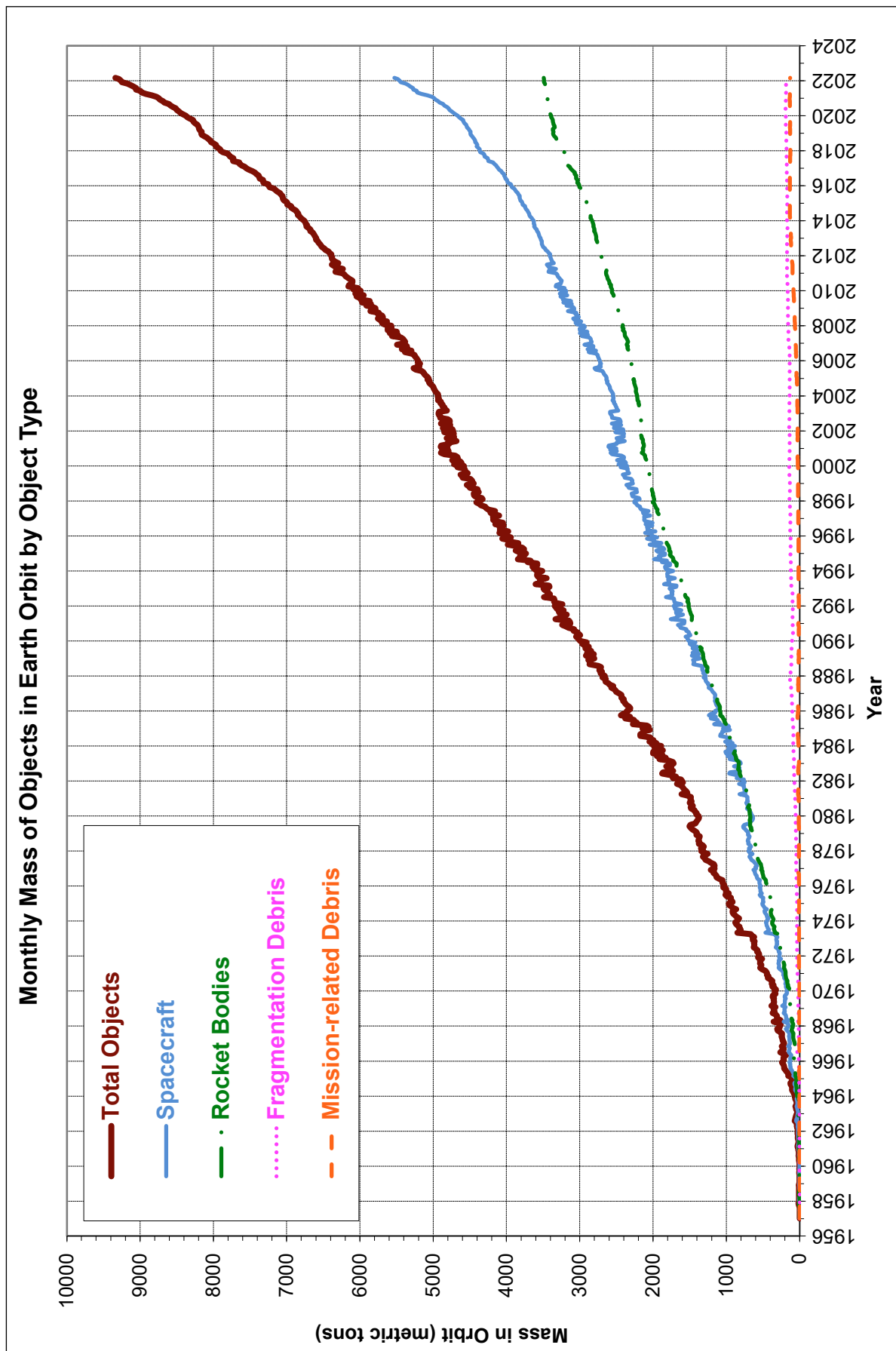


Effective numbers of objects per 10 km altitude bin between 200 and 2000 km altitude at four different epochs. These are objects, approximately 10 cm and larger, tracked by the Space Surveillance Network, including real objects with SSN numbers of 80,000 and greater. The increase from 2000 to 2007 was dominated by fragments generated from the Fengyun-1C antisatellite test conducted by China in 2007 and the accidental collision between Cosmos 2251 and the operational Iridium 33 spacecraft in 2009. The increase from 2010 to 2020 was driven by the initial build-up of the Starlink large constellation (120 Starlink spacecraft were launched from May to November 2019) and by the proliferation of CubeSats below about 650 km altitude. The increase from 2020 to 2022 continues to be driven by the Starlink and CubeSats below about 650 km altitude, with a new increase near 1200 km altitude driven by the OneWeb large constellation.

Monthly Effective Number of Objects in Earth Orbit



Monthly Effective Number of Objects in Earth Orbit by Orbital Regime cataloged by the U.S. Space Surveillance Network, except those with SSN numbers of 80,000 and greater. This chart displays the number of all objects in Earth orbit officially cataloged by the U.S. Space Surveillance Network. Low Earth orbit (LEO) includes resident space objects (RSOs) with altitudes within or crossing below 2,000 km; medium Earth orbit (MEO) RSOs with altitudes within or crossing the range from 2,000 km to 35,586 km; geosynchronous orbit (GEO) RSOs with altitudes within or crossing the range from 35,586 km to 35,986 km; and the remainder with altitudes within or crossing the range from 35,986 km to 600,000 km, referred to as Super-GEO. "Effective" number sums the fraction of each orbit that falls within the specified ranges. Cataloged objects without available orbital elements are excluded.



Monthly Mass of Objects in Earth Orbit by Object Type as of 3 May 2022. This chart displays the mass of all objects in Earth orbit officially cataloged by the U.S. Space Surveillance Network.

SATELLITE BOX SCORE

(as of 4 May 2022, cataloged by the
U.S. SPACE SURVEILLANCE NETWORK)

| Country/ Organization | Spacecraft* | Spent Rocket Bodies & Other Cataloged Debris | Total |
|--------------------------|-------------|---|--------------|
| CHINA | 529 | 3833 | 4362 |
| CIS | 1556 | 6707 | 8263 |
| ESA | 96 | 60 | 156 |
| FRANCE | 80 | 520 | 600 |
| INDIA | 107 | 115 | 222 |
| JAPAN | 207 | 111 | 318 |
| UK | 480 | 1 | 481 |
| USA | 4433 | 5209 | 9642 |
| OTHER | 1068 | 97 | 1165 |
| TOTAL | 8556 | 16653 | 25209 |

* active and defunct

Visit the NASA
Orbital Debris Program Office Website

www orbitaldebris jsc nasa gov

Technical Editor
Heather Cowardin, Ph.D.

Managing Editor
Debi Shoots

Correspondence can be sent to:

Robert Margetta
robert.j.margetta@nasa.gov

or to:
Nilufar Ramji
nilufar.ramji@nasa.gov

National Aeronautics and Space Administration
Lyndon B. Johnson Space Center
2101 NASA Parkway
Houston, TX 77058

www.nasa.gov
<https://orbitaldebris.jsc.nasa.gov/>

INTERNATIONAL SPACE MISSIONS

01 January 2022 – 31 March 2022

| Intl.* Designator | Spacecraft | Country/ Organization | Perigee Alt. (KM) | Apogee Alt. (KM) | Incl. (DEG) | Addnl. SC | Earth Orbital R/B | Other Cat. Debris |
|----------------------|------------------------|--------------------------|-------------------------|------------------------|----------------|--------------|-------------------------|-------------------------|
| 1998-067 | ISS dispensed payloads | Various | 413 | 422 | 51.6 | 9 | 0 | 4 |
| 2022-001A | STARLINK-3321 | US | 539 | 541 | 53.2 | 48 | 0 | 4 |
| 2022-002A | FOSSASAT2E2 | SPN | 504 | 524 | 97.5 | 105 | 0 | 0 |
| 2022-003B | TECHEDSAT 13 | SPN | 490 | 499 | 45.0 | 6 | 1 | 0 |
| 2022-004A | SHIYAN 13 (SY-13) | PRC | 357 | 1292 | 98.7 | 0 | 1 | 0 |
| 2022-005A | STARLINK-3366 | US | 539 | 541 | 53.2 | 48 | 0 | 4 |
| 2022-006A | USA 324 | US | 35783 | 35791 | 0.1 | 0 | 1 | 0 |
| 2022-006B | USA 325 | US | 35712 | 35720 | 0.1 | | | |
| 2022-007A | LT-1 O1A | PRC | 602 | 604 | 97.8 | 0 | 1 | 1 |
| 2022-008A | CSG-2 | IT | 621 | 624 | 97.9 | 0 | 0 | 0 |
| 2022-009A | USA 326 | US | 516 | 516 | 97.4 | 0 | 0 | 0 |
| 2022-010A | STARLINK-3XXX | US | 144 | 164 | 53.2 | 16 | 0 | 4 |
| 2022-011A | COSMOS 2553 | CIS | 1993 | 2000 | 67.1 | 0 | 0 | 0 |
| 2022-012A | ONEWEB-0410 | UK | 583 | 589 | 87.2 | 33 | 0 | 0 |
| 2022-013A | EOS-4 | IND | 527 | 529 | 97.5 | 0 | 1 | 0 |
| 2022-013B | INSPIRESAT-1 | IND | 518 | 532 | 97.6 | | | |
| 2022-013C | INS-2TD | IND | 517 | 530 | 97.6 | | | |
| 2022-014A | PROGRESS MS-19 | CIS | 415 | 422 | 51.6 | 0 | 1 | 0 |
| 2022-015A | CYGNUS NG-17 | US | 415 | 422 | 51.6 | 0 | 1 | 1 |
| 2022-016A | STARLINK-3528 | US | 538 | 541 | 53.2 | 45 | 0 | 4 |
| 2022-017A | STARLINK-3622 | US | 502 | 504 | 53.2 | 49 | 0 | 4 |
| 2022-018A | LT-1 O1B | PRC | 602 | 604 | 97.8 | 0 | 1 | 0 |
| 2022-019A | OBJECT A | PRC | 525 | 553 | 97.5 | 21 | | |
| 2022-020A | STRIX-BETA | JPN | 554 | 573 | 97.8 | 0 | 2 | 0 |
| 2022-021A | GOES 18 | US | 35782 | 35792 | 0.0 | 0 | 1 | 0 |
| 2022-022A | STARLINK-3542 | US | 538 | 542 | 53.2 | 46 | 0 | 4 |
| 2022-023A | OBJECT A | PRC | 480 | 513 | 63.5 | 6 | | |
| 2022-024A | NOUR 02 | IRAN | 488 | 515 | 58.3 | 0 | 1 | 0 |
| 2022-025A | STARLINK-3700 | US | 448 | 450 | 53.2 | 47 | 0 | 4 |
| 2022-026B | SPACEBEE-121 | US | 502 | 541 | 97.5 | 20 | 1 | 0 |
| 2022-027A | YAOGAN-34 02 | PRC | 1084 | 1096 | 63.4 | 0 | 1 | 0 |
| 2022-028A | SOYUZ MS-21 | CIS | 415 | 422 | 51.6 | 0 | 1 | 0 |
| 2022-029A | STARLINK-3537 | US | 333 | 339 | 53.2 | 52 | 0 | 4 |
| 2022-030A | MERIDIAN 10 | CIS | 975 | 39766 | 62.8 | 0 | 1 | 0 |
| 2022-030B | FREGAT R/B | CIS | 861 | 39592 | 62.8 | | | |
| 2022-031A | TK-2 | PRC | 585 | 605 | 97.8 | 0 | 1 | 0 |
| 2022-031B | PUJIANG 2 (PJ-2) | PRC | 586 | 606 | 97.8 | | | |
| 2022-032A | OBJECT A | PRC | 588 | 607 | 97.8 | 0 | 1 | 0 |
| 2022-032C | OBJECT C | PRC | 580 | 604 | 97.8 | | | |
| 2022-032D | OBJECT D | PRC | 579 | 604 | 97.8 | | | |

* Intl. = International; SC = Spacecraft; Alt. = Altitude; Incl. = Inclination; Addnl. = Additional; R/B = Rocket Bodies; Cat. = Cataloged

Notes: 1. Orbital elements are as of data cut-off date 31 March. 2. Additional spacecraft on a single launch may have different orbital elements. 3. Additional uncatalogued objects may be associated with a single launch.